https://doi.org/10.5194/egusphere-2022-315
Preprint. Discussion started: 13 July 2022

Retrievals of Precipitable Water Vapor and Aerosol Optical Depth from direct sun measurements with EKO MS711 and MS712 Spectroradiometers

Congcong Qiao[1,2], Song Liu[1,2], Juan Huo[1], Xihan Mu[3], Ping Wang[4], Shengjie Jia[5], Xuehua Fan[1], Minzheng Duan[1,2*]

[1]LAGEO, Institute of Atmospheric Physics, Chinese Academy of Sciences, Beijing, 100029, China
[2]College of Earth and Planetary Sciences, University of Chinese Academy of Sciences, Beijing, 100049, China
[3]State Key Laboratory of Remote Sensing Science, Beijing Normal University, Beijing, 100875, China
[4] Royal Netherlands Meteorological Institute (KNMI), De Bilt, the Netherlands
[5]Beijing Keytec Technology Co., Ltd., Beijing, 100102, China

Correspondence to: Minzheng Duan (dmz@mail.iap.ac.cn)

Abstract. Based on the strict radiative transfer algorithm, a new method is developed to derive the Precipitable Water Vapor (PWV) and Aerosol optical depth (AOD) from the ground-based measurements of direct sun irradiance. The attenuated direct irradiance from 300 nm to 1700 nm with FWHM of 6.5 nm are measured by a pair of grating spectroradiometers MS711 and MS712, located at the Institute of Atmospheric Physics, Chinese Academy of Sciences (39.98° N, 116.38° E), from June 2020 to March 2021. Compared to that of regular sun photometers such as CIMEL and POM, a strong water vapor absorption band near 1370 nm is introduced to derive PWV for the relatively dry atmosphere. The PWV and AOD inversion results obtained by EKO are compared with the synchronous data of CIMEL, and the two are highly consistent. The correlation coefficient, mean bias and standard deviation of PWV_{EKO} and PWV_{CIMEL} are 0.999, -0.027 cm (-3.57 %) and 0.054 cm (3.93 %) respectively, and the relative deviations of the differences between the two are slightly larger for drier air (PWV<5 mm) and lower solar elevation angle. The correlation coefficients of AOD_{EKO} and AOD_{CIMEL} at 380, 440, 500, 675, 870, 1020 nm are greater than 0.99, and the relative deviations are between -13.59 % and 9.37 %.

1 Introduction

Water vapor and aerosols are two key components of the atmosphere (Bojinski et al., 2014; IPCC, 2013), and the current accuracy of their indirect measurements from spaceborne instruments (Dubovik et al., 2019; Kaufman et al., 2002; Kokhanovsky, 2013) are unsatisfactory in evaluation of earth climate simulations and environment modelling (IPCC, 2021), often needing to be combined with ground-based measurements for higher accuracy retrievals (Li et al., 2019; WMO, 2016). As for PWV, ground observation methods include Global Positioning System (GPS), MicroWave radiation Profiler System (MWPS), sun photometers (CIMEL, POM, MFR), etc. GPS signals delayed by atmosphere can be used to obtain PWV at a relatively high time frequency globally, but the algorithm still needs to be improved for accuracy (Bevis et al., 1992; Wang et

https://doi.org/10.5194/egusphere-2022-315
Preprint. Discussion started: 13 July 2022

al., 2007). MWPS measures the radiation emitted from the atmosphere by microwaves, yields a vertical profile of water vapor, which can then be integrated to give PWV, where aerosols have little effect, but this measurement is very expensive (Güldner and Spänkuch, 2001; J. and Güldner, 2013). Solar photometers are easy to operate and economical to build observation network (Augustine et al., 2008; Wehrli, 2003), and are widely used to monitor water vapor and aerosols (Barreto et al., 2014; Cuevas Agulló et al., 2015; Kazadzis et al., 2014; Schmid et al., 1999). Among them, the CIMEL is the most popular one and used in the AErosol RObotic NETwork (AERONET) project (Holben et al., 1998), and China Aerosol Remote Sensing Network (CARSNET) (Che et al., 2016), Sun–Sky Radiometer Observation Network (SONET) (Li et al., 2018) etc. Similar instruments such as POM are deployed in the SKY radiometer NETwork (SKYNET) (Campanelli et al., 2012; Campanelli et al., 2014). Currently, AERONET is the most recognized ground-based observation network. Since the 1990s, NASA and PHOTOS have established more than 500 sites worldwide based on CIMEL sun photometer, which could provide PWV and aerosol optical properties through several narrow bands measurements in the visible and short-wave infrared, and the results are often used as reference to that obtained by other methods. Additionally, some scientists have attempted to retrieve PWV and AOD using spectral measurements. Estellés et al. (2006) used li-COR 1800 spectroradiometer to retrieve AOD, their results showed the differences with CIMEL of 0.01-0.03 and 0.02-0.05 in the ultraviolet and visible band, respectively. Cachorro et al. (2009) compared AOD obtained by li-COR and sun photometer and found the differences of AOD within 0.02 in the 440-1200 nm spectral range. The results of PWV and AOD from spectral measurements with Precision Solar spectroRadiometer (PSR) showed a standard deviation of 0.18 cm for PWV and an overestimation of 0.01 to 0.03 for AOD compared to CIMEL, and the PWV given by the integration of single water vapor band near 940 nm has great variability at different wavelengths (Kazadzis et al., 2018a; Kazadzis et al., 2018b; Kazadzis et al., 2014; Raptis et al., 2018). García et al. (2020) and García et al. (2021) retrieved PWV and AOD using the EKO MS711 spectroradiometer at Izana Observatory in Spain, and compared them with CIMEL, showing that PWV has a mean bias of 0.033 cm, and the AOD is basically consistent.

A method of simple Lambert-Beer law was used to retrieve AOD and a three-parameter formula proposed by Ingold et al. (2000) was used for PWV with measurements of 940 nm water vapor band in the above mentioned publications. Since the three-parameter formulation method is very sensitive to the instrument slit function, air quality and wavelength, a spectral fitting algorithm is proposed to derive the PWV. In this work, Direct Normal solar Irradiance (DNI) at 300-1700 nm was measured with EKO MS711 and MS712 spectroradiometers, then AOD and PWV were retrieved and compared to CIMEL, additionally, the water vapor absorption band near 1370 nm was also used to obtain PWV, which was expected to improve the water vapor retrieval efficiency in dry environment.

2 Instruments and data

The grating spectroradiometers MS711 and MS712 are designed and developed by EKO INSTRUMENTS and can be used to measure the attenuation of direct solar beams in the range of 300-1700 nm, with a high time resolution of 1 minute. The average wavelength interval is 0.4 nm and 2.0 nm, respectively, the Full Width at Half Maximum (FWHM) is less than 7 nm,

https://doi.org/10.5194/egusphere-2022-315
Preprint. Discussion started: 13 July 2022

the wavelength accuracy is ±0.2 nm, the temperature is controlled within 25±2 ℃ and -5±0.5 ℃, respectively, the exposure time is 10-5000 ms, and the full Field Of View angle (FOV) is 5°. The main specifications related to the EKO instruments are listed in Table 1.

CE318 is a narrow-band photometer developed by CIMEL Electronique in France, which can directly measure the radiance of the sun and the sky. Measurements are usually made every 10-15 minutes at 340, 380, 440, 500, 675, 870, 940, 1020 and 1640 nm through rotating filter wheels. The spectral resolution of the instrument is 2 nm, 10 nm and 40 nm in the ultraviolet band, visible band and near-infrared band (Schmid et al., 1999), respectively. The FOV of CE318 is about 1.2° and calibrated annually.

The instruments are collocated in the Institute of Atmospheric Physics, Chinese Academy of Science, Beijing (39.98° N, 116.38° E, 92 m a.s.l, Fig. 1), in North of China, where is a relatively dry location, and most of the precipitation happens in summer. The data used here are collected from June 2020 to March 2021, and data level 1.5 of AERONET (https://AERONET.gsfc.nasa.gov/) are used for comparison.

3 Inversion Method

Cloud influences need to be avoided before performing the inversion work. Considering that the changes of clouds in a short time are usually more drastic than that of aerosols and the temporal resolution of EKO spectroscopic measurements is relatively high at 1 min. We refer to the method developed by Alexandrov et al. (2004) to judge whether there is cloud influence by the variability of EKO radiation measurements at 870 nm over a 10 minutes period, so as to screen out the measurement data without cloud influence for the following water vapor and aerosol inversion.

3.1 PWV inversion

Figure 2 shows multiple water vapor absorption windows in the spectral curves measured by EKO spectroradiometers. Figure 3 shows the theoretical transmittance curves for Rayleigh scattering, aerosols, and water vapor from 300 nm to 1700 nm calculated by MODTRAN 4.3 (Larar et al., 1999) at 0° solar zenith angle. WMO (2005) recommends the use of 719, 817 and 946 nm central wavelengths to obtain PWV, which are marked with the grey arrows in Fig. 3. Ingold et al. (2000) compared the water vapor inversion results of these wavelengths and found that 946 nm is of the most suitable for PWV retrieval. The water vapor data provided by AERONET are also obtained by the band near 946 nm (Smirnov et al., 2004). However, as demonstrated in Fig. 3, the transmittance at 946 nm turns to be less sensitive to water vapor as the air becomes drier, while the water vapor absorption remains strong around 1370 nm , based on this, the water vapor absorption window of 1350-1450 nm was considered for PWV inversion in very dry atmosphere.

The transmittance $T(\lambda)$ of the whole atmosphere along the sun's direction can be expressed by the Bouguer-Lambert-Beer law (Swinehart and D., 1962):

https://doi.org/10.5194/egusphere-2022-315
Preprint. Discussion started: 13 July 2022

$$T(\lambda) = \frac{I(\lambda)}{I_0(\lambda)} = e^{-m_r\tau_r(\lambda) - m_a\tau_a(\lambda) - m_g\tau_g(\lambda)} , \quad (1)$$

where $I(\lambda)$ is DNI recorded by the EKO instruments at wavelength λ, $I_0(\lambda)$ is the solar radiance at the top of the atmosphere, m and τ is the airmass and optical thickness, respectively, the subscript r, a and g stands for the contribution of Rayleigh, aerosols and other atmospheric gases, respectively (Bodhaine et al., 1999; Gueymard, 2001; Hansen and Travis, 1974). In the water vapor absorption band near 940 nm and 1370 nm, the absorption of other gases except water vapor can be neglectable, the subscription g in above equation is replaced by w , which means water vapor, and Eq. (1) can be rewritten as:

$$\frac{I(\lambda)}{I_0(\lambda)} = e^{-m_r\tau_r(\lambda) - m_a\tau_a(\lambda)} T_w(\lambda) , \quad (2)$$

$$T_w(\lambda) = \frac{I(\lambda)}{I_0(\lambda) e^{-m_r\tau_r(\lambda) - m_a\tau_a(\lambda)}} = \frac{I(\lambda)}{I_1(\lambda)} , \quad (3)$$

where T_w is the transmittance within the water vapor band, $I_1(\lambda)$ is the radiance without absorption of water vapor:

$$I_1(\lambda) = I_0(\lambda) e^{-m_r\tau_r(\lambda) - m_a\tau_a(\lambda)} , \quad (4)$$

$I_1(\lambda)$ can be approximated by the interpolation of the base-line points outside of the water vapor band as the dotted lines shown in Fig. 4. The average transmittance within the water vapor band between λ_1 and λ_2 can be expressed as:

$$T_{w,\Delta\lambda} = \frac{1}{\Delta\lambda} \int_{\lambda_1}^{\lambda_2} \frac{I(\lambda)}{I_1(\lambda)} d\lambda , \quad (5)$$

$T_{w,\Delta\lambda}$ can be given both by EKO spectrometers MS711 and MS712 denoted as T_w^E, or by radiative transfer model, denoted as T_w^m, here the MODTRAN version 4.3 is used.

T_w^M was simulated with first guess of PWV and then the differences between T_w^M and T_w^E was calculated:

$$\Delta = T_w^E - T_w^M , \quad (6)$$

Recalculating Eq. (6) by increasing or decreasing PWV depending on that Δ is positive or negative, the final value of PWV was given by iteration of Eq. (6) as Δ becomes smaller than a criteria value:

$$\Delta \rightarrow min\left(\left|T_{w,\Delta\lambda}^E - T_{w,\Delta\lambda}^M\right|\right) \Longrightarrow PWV , \quad (7)$$

The above algorithm was tested separately for both Band1 (900-990 nm) and Band2 (1340-1450 nm), respectively, and 1000 spectral curves simulated by MODTRAN were used for the test. When simulating spectral curves, the US standard atmospheric model was selected, regardless of clouds and aerosols, randomly inputted PWV of 0-0.5 cm and solar zenith angle of 10°-45°, and superimposed -1 %-+1 % noise on the simulated curves. The inversion test results using two bands demonstrated in Fig. 5, which show that retrievals from the band near 1370 nm is more applicable for dry atmosphere than that from the band near 940 nm.

3.2 AOD inversion

After PWV is given, the spectral variation of AOD is derived according to Bouguer-Lambert-Beer law:

$$AOD = ln\left(I_0(\lambda)\right) - ln\left(I(\lambda)\right) - \tau_r - \tau_g , \quad (8)$$

$$\tau_r = p/p_0 \times 0.0088\lambda^{-4.05} , \quad (9)$$

https://doi.org/10.5194/egusphere-2022-315
Preprint. Discussion started: 13 July 2022

$$\tau_g = \tau_{H_2O} + \tau_{N_2O} + \tau_{O_2} + \tau_{O_3} + \cdots , \quad (10)$$

To mitigate the absorption of gases other than water vapor, the wavelengths are carefully selected, only the wavelengths that have very small gas absorption are used for AOD retrieval. The Rayleigh scattering τ_r is given by Eq. (9) (Ramachandran et al., 1994), p_0=1013.25 hPa, p is provided by meteorological observation located in IAP, τ_{H_2O} is obtained from PWV inversion as Sect. 3.1.

4 Results

About 10 months measurements, from June 2020 to March 2021, of MS711 and MS712 on top of IAP's building are used to derive the PWV and AOD, the CE318 results of the same time and same location are used as reference, the number of matching data points is 5008. The mean deviation and variance between the results of the two instruments are given by:

$$\overline{X} = \frac{1}{n}\sum_i \left(X^i_{EKO} - X^i_{cimel}\right) , \quad (11)$$

$$\delta_X = \sqrt{\frac{1}{n}\sum_i \left(X^i_{EKO} - X^i_{cimel}\right)^2} , \quad (12)$$

where X is either PWV or AOD, the subscript stands for EKO or CIMEL.

The retrievals of PWV using the band near 940 nm from the two instruments are shown in Fig. 6. It reveals that the retrievals from EKO have a high consistency with that from CIMEL, the correlation coefficient is of 0.999, the mean bias and the standard deviation are of -0.027 cm (-3.57 %) and 0.054 cm (3.93 %), respectively, the relative differences for 95 % of the retrievals are between -0.114 and 0.042, and the differences have solar elevation angle dependency, the lower sun position, the larger difference, which is explained by the increase of the instrument-related uncertainty at higher SZA. In addition, as can be seen from Table 2, the relative deviations of the PWV obtained by Band1 (near 940 nm) changed from -2.67 % to -4.90 % with decreasing water vapor content (PWV < 0.5 cm), therefore, we speculate that the uncertainty of PWV inversion under dry conditions may increase.

Figure 7 shows the water vapor retrievals of Band1 (near 940 nm) and Band2 (near 1370 nm) for dry atmosphere, here we say PWV_{CIMEL} < 0.5 cm, their statistics are also presented in Table 2. The results of BAND1 are relatively higher than those of BAND2, which is consistent with the simulation results in Fig. 4, indicating that although the PWV retrievals of the band near 940 nm are closer to AERONET, the PWV inversion using the band near 1370 nm may be more accurate for dry atmosphere.

An example of the AOD vs. wavelength is illustrated in Fig. 8, it shows the AOD derived from EKO is highly close to the data of AERONET-CIMEL in this case. To further evaluate the differences between AOD_{EKO} and AOD_{CIMEL}, the AOD_{EKO} in the corresponding bands (380, 440, 500, 675, 870, 1020 nm) of the CIMEL was compared and analysed, as displayed in Fig. 9, AOD retrievals from the two instruments are very similar, and Table 3 lists the specific statistics.

The correlation coefficients are all higher than 0.99, the relative differences are between -13.59 % and 9.37 %. Further analysis found that the AOD differences in the visible band are relatively small, especially at 500 nm the MB and RMSE are -0.003

https://doi.org/10.5194/egusphere-2022-315
Preprint. Discussion started: 13 July 2022

(0.69 %) and 0.021 (7.46 %), respectively, while relatively large in the near-infrared band, particularly at 870nm, MB and RMSE are -0.014 (-13.59 %) and 0.021 (20.01 %), respectively.

Figure 10 plots the difference variation of AOD with that of CIMEL for 380 nm and 675 nm. It shows obvious underestimation trend, especially for the 380nm, which is reasonable since current AOD inversion algorithm neglect the forward scattering that can lead to underestimation of AOD (Sinyuk et al., 2012). The FOV of MS711 and MS712 is 5°, which is double that of the radiometer for AOD recommended by WMO and four times that of CIMEL, therefore, the forward scattered photons received by MS711 and MS712 are also bigger than CIMEL, especially for heavy aerosol loading atmosphere and shorter wavelengths. The forward scattering correction will be considered in the next version of the algorithm.

5 Summary and Conclusions

The water vapor absorption band near 940 nm is currently used to derive the PWV, and aerosol optical depth is given at several wavelengths separately from sun photometer. Combined with the advantage of EKO instruments that can measure the direct normal solar irradiance at 300-1700 nm, the water vapor band near 1370 nm is also used to derive the PWV for dry atmosphere and then spectral AOD is retrieved. Different from the three-parameter method, the retrieval algorithm is based on MODTRAN version 4.3. Data measured by EKO MS711 and MS712 at IAP from June 2020 to March 2021 are used for inverting PWV and spectral AOD, and the results are compared with those from co-located CIMEL.

The PWV retrieved from both instruments with the band near 940 nm are in good agreement, the correlation coefficient is 0.999, the mean bias, root mean square error and standard deviation are -0.027 cm (-3.57 %), 0.061 cm (5.31 %) and 0.054 cm (3.93 %), respectively. However, for dry atmosphere with PWV<0.5 cm, retrievals by using the band near 1370 nm may be more accurate than that by using the band near 940 nm according to the results of simulated inversion.

The AOD retrieved from EKO instruments also agree well with that from CIMEL, the correlation coefficients are greater than 0.99, the mean bias are between -0.016 and 0.008. Due to the large FOV of the EKO instruments and the current algorithm ignoring the contribution of forward scattering, the AOD retrievals from EKO are often slightly underestimated, especially for heavy aerosol loading atmosphere and shorter wavelengths, which will be considered in future version.

Data availability

Data used in this study are available from the corresponding author upon request (dmz@mail.iap.ac.cn).

https://doi.org/10.5194/egusphere-2022-315
Preprint. Discussion started: 13 July 2022

Author contributions

M. Duan and C. Qiao determined the main goal of this study. C. Qiao carried it out, analysed the data, and prepared the paper with contributions from all co-authors. S. Jia provided instrumental support. P. Wang and J. Huo provided guidance on algorithmic procedures.

Competing interests

The authors declare that they have no conflict of interest.

Acknowledgements

This research is supported by the National Natural Science Foundation of China (Grant No. 42030107 and No. 42175150). We also thank all the teachers and students who participated in the discussion about this work.

References

Alexandrov, M. D., Marshak, A., Cairns, B., Lacis, A. A., and Carlson, B. E.: Automated cloud screening algorithm for MFRSR data, Geophys. Res. Lett., 31, https://doi.org/https://doi.org/10.1029/2003GL019105, 2004.

Augustine, J. A., Hodges, G. B., Dutton, E. G., Michalsky, J. J., and Cornwall, C. R.: An aerosol optical depth climatology for NOAA's national surface radiation budget network (SURFRAD), J. Geophys. Res., 113, https://doi.org/10.1029/2007jd009504, 2008.

Barreto, A., Cuevas, E., Pallé, P., Romero, P. M., Guirado, C., Wehrli, C. J., and Almansa, F.: Recovering long-term aerosol optical depth series (1976–2012) from an astronomical potassium-based resonance scattering spectrometer, Atmos. Meas. Tech., 7, 4093-4121, https://doi.org/10.5194/amt-7-4103-2014, 2014.

Bevis, M., Businger, S., Herring, T. A., Rocken, C., Anthes, R. A., and Ware, R. H.: GPS meteorology: Remote sensing of atmospheric water vapor using the global positioning system, J. Geophys. Res.: Atmos., 97, 15787-15801, https://doi.org/10.1029/92JD01517, 1992.

Bodhaine, B. A., Wood, N. B., Dutton, E. G., and Slusser, J. R.: On Rayleigh Optical Depth Calculations, J. Atmos. Oceanic Technol., 16, 1854-1861, https://doi.org/10.1175/1520-0426(1999)016<1854:Orodc>2.0.Co;2, 1999.

Bojinski, S., Verstraete, M., Peterson, T. C., Richter, C., Simmons, A., and Zemp, M.: The Concept of Essential Climate Variables in Support of Climate Research, Applications, and Policy, Bull. Am. Meteorol. Soc., 95, 1431-1443, https://doi.org/10.1175/bams-d-13-00047.1, 2014.

https://doi.org/10.5194/egusphere-2022-315
Preprint. Discussion started: 13 July 2022

Cachorro, V. E., Berjon, A., Toledano, C., Mogo, S., Prats, N., Frutos, M. D., Vilaplana, J. M., Sorribas, M., Morena, B. A. D. L., and Groebner, J.: Detailed Aerosol Optical Depth Intercomparison between Brewer and Li-Cor 1800 Spectroradiometers and a Cimel Sun Photometer, J. Atmos. Oceanic Technol., 26, 1558-1571, https://doi.org/10.1175/2009JTECHA1217.1, 2009.

Campanelli, M., Estelles, V., Smyth, T., Tomasi, C., and Nakajima, T.: Monitoring of Eyjafjallajoekull volcanic aerosol by the new European SkyRad users (ESR) sun-sky radiometer network, Atmos. Environ., 48, 33-45, https://doi.org/10.1016/j.atmosenv.2011.09.070, 2012.

Campanelli, M., Nakajima, T., Khatri, P., Takamura, T., Uchiyama, A., Estelles, V., Liberti, G. L., and Malvestuto, V.: Retrieval of characteristic parameters for water vapour transmittance in the development of ground-based sun–sky radiometric measurements of columnar water vapour, Atmos. Meas. Tech., 7, 1075-1087, https://doi.org/10.5194/amt-7-1075-2014, 2014.

Che, H., Gui, K., Chen, Q., Zheng, Y., Yu, J., Sun, T., Zhang, X., and Shi, G.: Calibration of the 936 nm water-vapor channel for the China aerosol remote sensing NETwork (CARSNET) and the effect of the retrieval water-vapor on aerosol optical property over Beijing, China, Atmos. Pollut. Res., 7, 743-753, https://doi.org/10.1016/j.apr.2016.04.003, 2016.

Cuevas Agulló, E., Milford, C., and Tarasova, O.: Izaña Atmospheric Research Center. Activity Report 2012-2014, https://doi.org/10.31978/281-15-004-2, 2015.

Dubovik, O., Li, Z., Mishchenko, M. I., Tanré, D., Karol, Y., Bojkov, B., Cairns, B., Diner, D. J., Espinosa, W. R., Goloub, P., Gu, X., Hasekamp, O., Hong, J., Hou, W., Knobelspiesse, K. D., Landgraf, J., Li, L., Litvinov, P., Liu, Y., Lopatin, A., Marbach, T., Maring, H., Martins, V., Meijer, Y., Milinevsky, G., Mukai, S., Parol, F., Qiao, Y., Remer, L., Rietjens, J., Sano, I., Stammes, P., Stamnes, S., Sun, X., Tabary, P., Travis, L. D., Waquet, F., Xu, F., Yan, C., and Yin, D.: Polarimetric remote sensing of atmospheric aerosols: Instruments, methodologies, results, and perspectives, J. Quant. Spectrosc. Radiat. Transfer, 224, 474-511, https://doi.org/10.1016/j.jqsrt.2018.11.024, 2019.

Estellés, V., Utrillas, M. P., Martínez-Lozano, J. A., Alcántara, A., Alados-Arboledas, L., Olmo, F. J., Lorente, J., de Cabo, X., Cachorro, V., Horvath, H., Labajo, A., Sorribas, M., Díaz, J. P., Díaz, A. M., Silva, A. M., Elías, T., Pujadas, M., Rodrigues, J. A., Cañada, J., and García, Y.: Intercomparison of spectroradiometers and Sun photometers for the determination of the aerosol optical depth during the VELETA-2002 field campaign, J. Geophys. Res., 111, https://doi.org/10.1029/2005jd006047, 2006.

García, R. D., Cuevas, E., Barreto, Á., Cachorro, V. E., Pó, M., Ramos, R., and Hoogendijk, K.: Aerosol retrievals from the EKO MS-711 spectral direct irradiance measurements and corrections of the circumsolar radiation, Atmos. Meas. Tech., 13, 2601-2621, https://doi.org/10.5194/amt-13-2601-2020, 2020.

García, R. D., Cuevas, E., Cachorro, V. E., García, O. E., Barreto, Á., Almansa, A. F., Romero-Campos, P. M., Ramos, R., Pó, M., Hoogendijk, K., and Gross, J.: Water Vapor Retrievals from Spectral Direct Irradiance Measured with an EKO MS-711 Spectroradiometer—Intercomparison with Other Techniques, Remote Sens., 13, https://doi.org/10.3390/rs13030350, 2021.

Gueymard, C. A.: Parameterized transmittance model for direct beam and circumsolar spectral irradiance, Sol. Energy, 71, 325-346, https://doi.org/10.1016/S0038-092X(01)00054-8, 2001.

https://doi.org/10.5194/egusphere-2022-315
Preprint. Discussion started: 13 July 2022

Güldner, J. and Spänkuch, D.: Remote Sensing of the Thermodynamic State of the Atmospheric Boundary Layer by Ground-Based Microwave Radiometry, J. Atmos. Oceanic Technol., 18, 925-933, https://doi.org/10.1175/1520-0426(2001)018<0925:Rsotts>2.0.Co;2, 2001.

Hansen, J. E. and Travis, L. D.: Light scattering in planetary atmospheres, Space Sci. Rev., 16, 527-610, https://doi.org/10.1007/BF00168069, 1974.

Holben, B. N., Eck, T. F., Slutsker, I., Tanré, D., Buis, J. P., Setzer, A., Vermote, E., Reagan, J. A., Kaufman, Y. J., and Nakajima, T.: AERONET—A Federated Instrument Network and Data Archive for Aerosol Characterization, Remote Sens. Environ., 66, 1-16, https://doi.org/10.1016/S0034-4257(98)00031-5, 1998.

Ingold, T., Schmid, B., Mätzler, C., Demoulin, P., and Kämpfer, N.: Modeled and empirical approaches for retrieving columnar water vapor from solar transmittance measurements in the 0.72, 0.82, and 0.94 μm absorption bands, J. Geophys. Res.: Atmos., 105, 24327-24343, https://doi.org/10.1029/2000jd900392, 2000.

IPCC: The Physical Science Basis. Intergovernmental Panel on Climate Change, https://doi.org/10.1017/CBO9781107415324, 2013.

IPCC: Climate Change 2021: The Physical Science Basis. Contribution of Working Group I to the Sixth Assessment Report of the Intergovernmental Panel on Climate Change, https://doi.org/10.1017/9781009157896, 2021.

J. and Güldner: A model-based approach to adjust microwave observations for operational applications: results of a campaign at Munich Airport in winter 2011/2012, Atmos. Meas. Tech., 6, 2879-2891, https://doi.org/10.5194/amt-6-2879-2013, 2013.

Kaufman, Y. J., Tanré, D., and Boucher, O.: A satellite view of aerosols in the climate system, Nature, 419, 215-223, https://doi.org/10.1038/nature01091, 2002.

Kazadzis, S., Kouremeti, N., Diémoz, H., Gröbner, J., and Wehrli, C.: Results from the Fourth WMO Filter Radiometer Comparison for aerosol optical depth measurements, Atmos. Chem. Phys., 1-27, https://doi.org/10.5194/acp-2017-1105, 2018a.

Kazadzis, S., Kouremeti, N., Nyeki, S., Gröbner, J., and Wehrli, C.: The World Optical Depth Research and Calibration Center (WORCC) quality assurance and quality control of GAW-PFR AOD measurements, Geosci. Instrum. Method. Data Syst., 7, 39-53, https://doi.org/10.5194/gi-7-39-2018, 2018b.

Kazadzis, S., Veselovskii, I., Amiridis, V., Gr?Bner, J., Suvorina, A., Nyeki, S., Gerasopoulos, E., Kouremeti, N., Taylor, M., and Tsekeri, A.: Aerosol microphysical retrievals from precision filter radiometer direct solar radiation measurements and comparison with AERONET, Atmos. Meas. Tech., 7, 2013– 2025, https://doi.org/10.5194/amt-7-2013-2014, 2014.

Kokhanovsky, A. A.: Remote sensing of atmospheric aerosol using spaceborne optical observations, Earth Sci. Rev., 116, 95-108, https://doi.org/10.1016/j.earscirev.2012.10.008, 2013.

Larar, A. M., Berk, A., Anderson, G. P., Bernstein, L. S., Acharya, P. K., Dothe, H., Matthew, M. W., Adler-Golden, S. M., Chetwynd, J. J. H., Richtsmeier, S. C., Pukall, B., Allred, C. L., Jeong, L. S., and Hoke, M. L.: MODTRAN4 radiative transfer modeling for atmospheric correction, Optical Spectroscopic Techniques and Instrumentation for Atmospheric and Space Research III, https://doi.org/10.1117/12.366388, 1999.

https://doi.org/10.5194/egusphere-2022-315
Preprint. Discussion started: 13 July 2022

Li, C., Li, J., Xu, H., Li, Z., Xia, X., and Che, H.: Evaluating VIIRS EPS Aerosol Optical Depth in China: An intercomparison against ground-based measurements and MODIS, J. Quant. Spectrosc. Radiat. Transfer, 224, 368-377, https://doi.org/10.1016/j.jqsrt.2018.12.002, 2019.

Li, Z. Q., Xu, H., Li, K. T., Li, D. H., Xie, Y. S., Li, L., Zhang, Y., Gu, X. F., Zhao, W., Tian, Q. J., Deng, R. R., Su, X. L., Huang, B., Qiao, Y. L., Cui, W. Y., Hu, Y., Gong, C. L., Wang, Y. Q., Wang, X. F., Wang, J. P., Du, W. B., Pan, Z. Q., Li, Z. Z., and Bu, D.: Comprehensive Study of Optical, Physical, Chemical, and Radiative Properties of Total Columnar Atmospheric Aerosols over China: An Overview of Sun–Sky Radiometer Observation Network (SONET) Measurements, Bull. Am. Meteorol. Soc., 99, 739-755, https://doi.org/10.1175/bams-d-17-0133.1, 2018.

Ramachandran, S., Jayaraman, A., Acharya, Y., and Subbaraya, B.: Features of aerosol optical depths over Ahmedabad as observed with a Sun-tracking photometer, Beitr. Phys. Atmosph., 67, 1994.

Raptis, P.-I., Kazadzis, S., Gröbner, J., Kouremeti, N., Doppler, L., Becker, R., and Helmis, C.: Water Vapor Retrieval using the Precision Solar Spectroradiometer, Atmos. Meas. Tech., 1143–1157, https://doi.org/10.5194/amt-2017-370, 2018.

Schmid, B., Michalsky, J., Halthore, R., Beauharnois, M., Harrison, L., Livingston, J., Russell, P., Holben, B., Eck, T., and Smirnov, A.: Comparison of aerosol optical depth from four solar radiometers during the fall 1997 ARM intensive observation period, Geophys. Res. Lett., 26, 2725-2728, https://doi.org/10.1029/1999gl900513, 1999.

Sinyuk, A., Holben, B. N., Smirnov, A., Eck, T. F., Slutsker, I., Schafer, J. S., Giles, D. M., and Sorokin, M.: Assessment of error in aerosol optical depth measured by AERONET due to aerosol forward scattering, Geophys. Res. Lett., 39, 23806, https://doi.org/10.1029/2012gl053894, 2012.

Smirnov, A., Holben, B., Lyapustin, A., Slutsker, I., and Eck, T.: AERONET processing algorithms refinement, AERONET Workshop, El Arenosillo, Spain, 10-14, 291795812, 2004.

Swinehart and D., F.: The Beer-Lambert Law, J. Chem. Educ., 39, 333, https://doi.org/10.1021/ed039p333, 1962.

Wang, J., Zhang, L., Dai, A., Van Hove, T., and Van Baelen, J.: A near-global, 2-hourly data set of atmospheric precipitable water from ground-based GPS measurements, J. Geophys. Res., 112, https://doi.org/10.1029/2006jd007529, 2007.

Wehrli, C.: Calibrations of filter radiometers for determination of atmospheric optical depth, Metrologia, 37, 419, https://doi.org/10.1088/0026-1394/37/5/16, 2003.

WMO: WMO/GAW Experts Workshop on a Global Surface-Based Network for Long Term Observations of Column Aerosol Optical Properties, GAW Report No. 162, WMO TD No. 1287, available at: https://library.wmo.int/doc_num.php?explnum_id=9299 (last access: 6 May 2022), 2005.

WMO: GAW Report-No 231, Fourth WMO Filter Radiometer Comparison (FRC-IV), Davos, Switzerland, 28 September–16 October 2015, WMO, available at: https://library.wmo.int/doc_num.php?explnum_id=3369 (last access: 6 May 2022), 2016.

https://doi.org/10.5194/egusphere-2022-315
Preprint. Discussion started: 13 July 2022

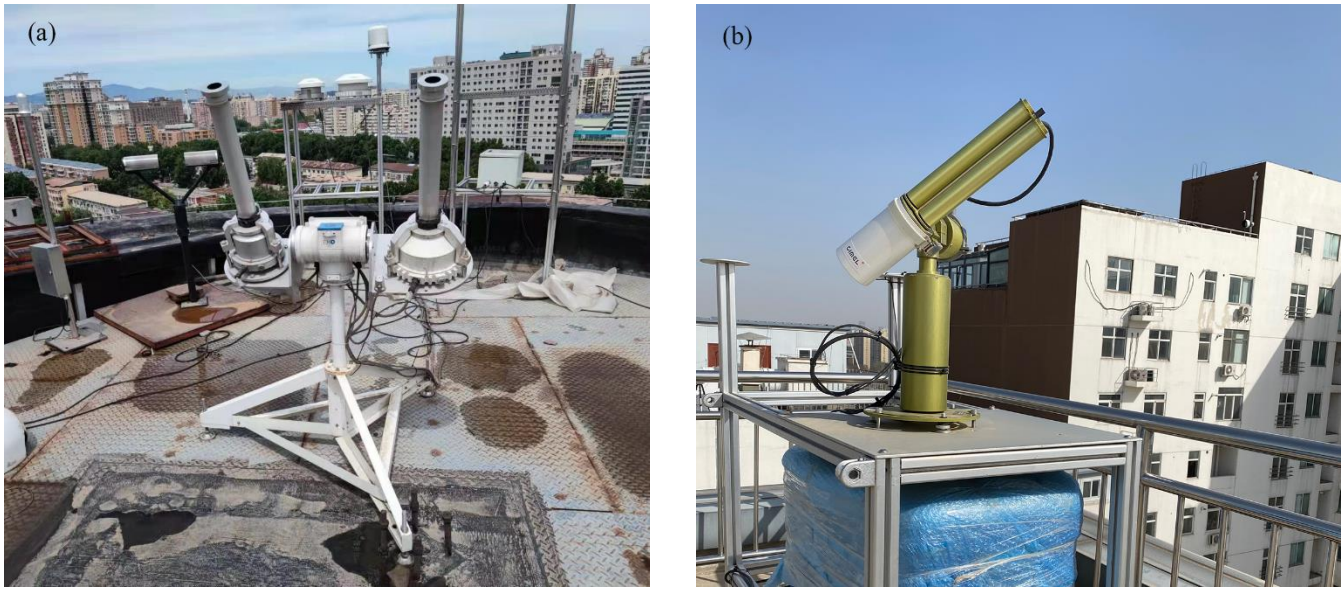

Figure 1. The EKO spectroradiometers (a) and CIMEL photometer (b) are co-located at the top of IAP's building.

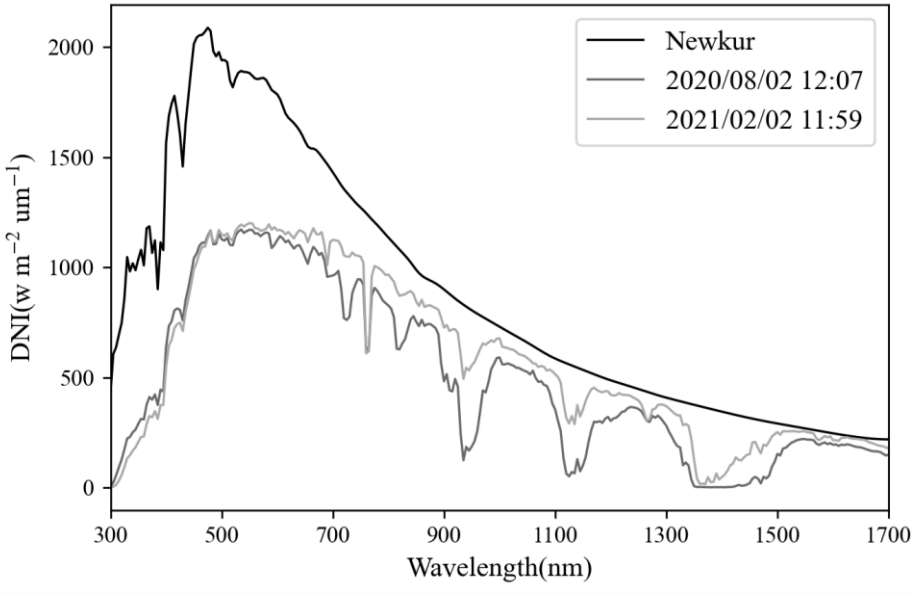

Figure 2. Direct normal irradiance(DNI) measured with the EKO MS-711 and MS712 spectroradiometers on 02 August 2020 (12:07 UTC+8) and 02 February 2021 (11:59 UTC+8) at IAP, the black curve represents solar irradiance at the top of the atmosphere.

https://doi.org/10.5194/egusphere-2022-315
Preprint. Discussion started: 13 July 2022

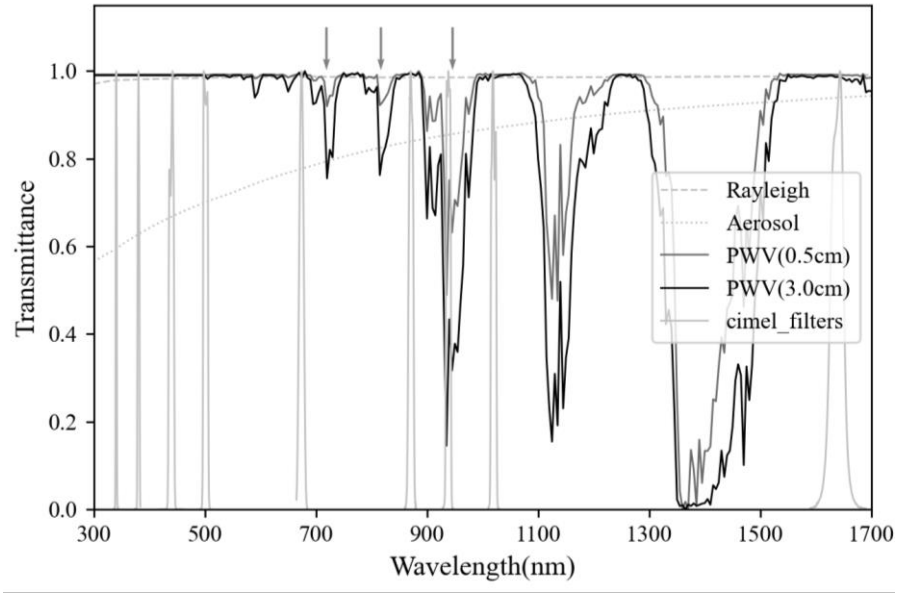

Figure 3. The spectrum response curves of CIMEL photometer's filter wheels, and the transmittance of water vapor, aerosols and Rayleigh scattering in the spectral region of 300–1700 nm, which are calculated by MODTRAN 4.3 at SZA=0°, PWV=0.5 cm, PWV=3.0 cm and Boundary Aerosol Model=Rural extinction, VIS=5 km. The wavelengths pointed by the grey arrows represent WMO recommendations for PWV retrieval.

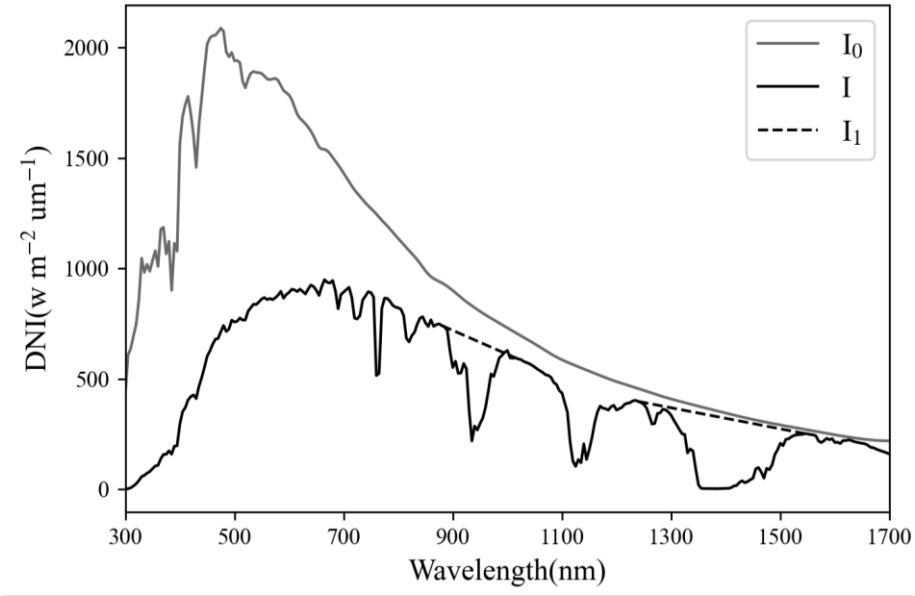

Figure 4. Direct normal solar irradiance reaching the surface, I, the irradiance after removing water vapor absorption, I_1, and the solar irradiance at the top of the atmosphere, I_0.

https://doi.org/10.5194/egusphere-2022-315
Preprint. Discussion started: 13 July 2022

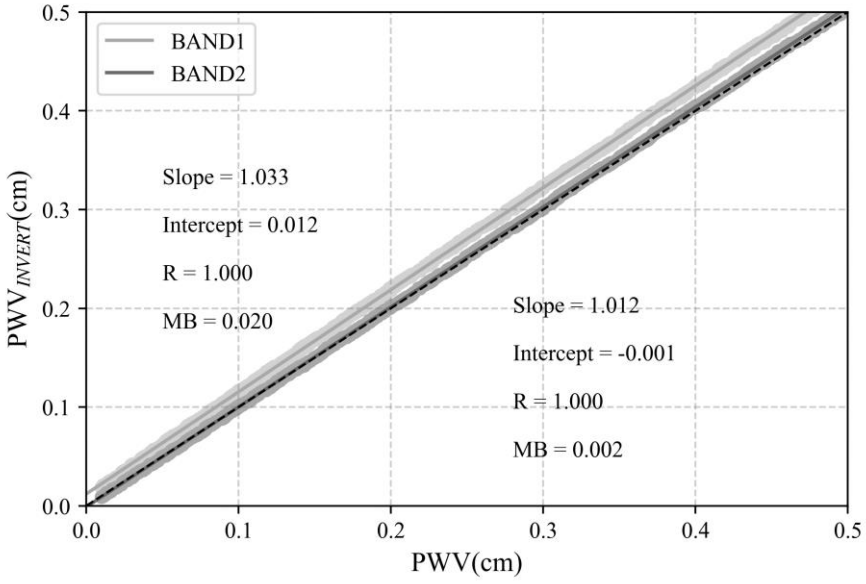

325 **Figure 5. The comparison between the water vapor inversions (PWV_{INVERT}) obtained by BAND1 and BAND2 of simulated spectrums and the real values (PWV).**

330

335

340

https://doi.org/10.5194/egusphere-2022-315
Preprint. Discussion started: 13 July 2022

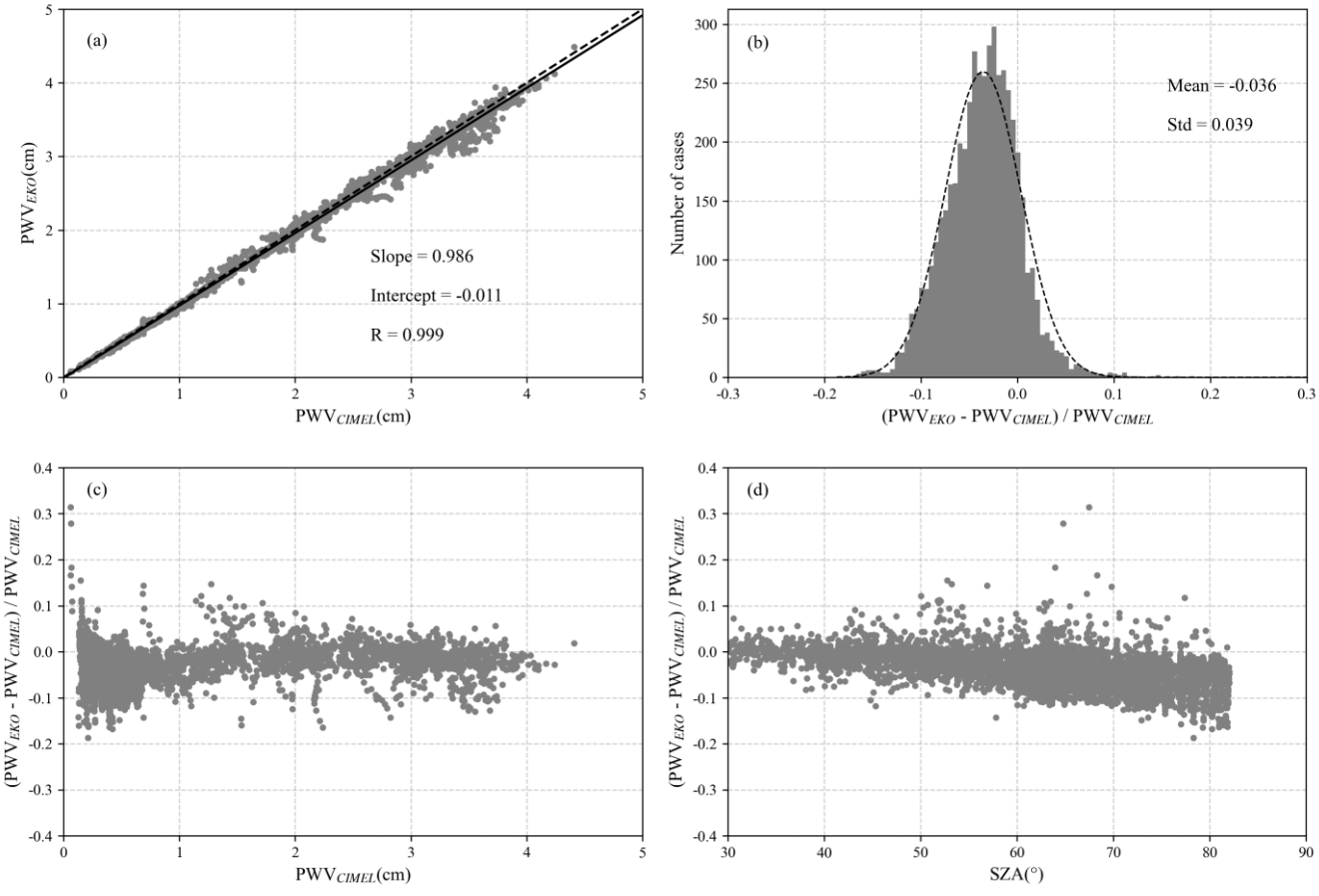

Figure 6. PWV retrievals from EKO using the spectral approach in the 880–1000 nm region compared to the synchronous data of CIMEL for the measuring period (a), histogram of relative difference among PWV_{EKO} and PWV_{CIMEL} (b), and the relative difference plotted against PWV_{CIMEL} (c) and solar zenith angle (d).

https://doi.org/10.5194/egusphere-2022-315
Preprint. Discussion started: 13 July 2022

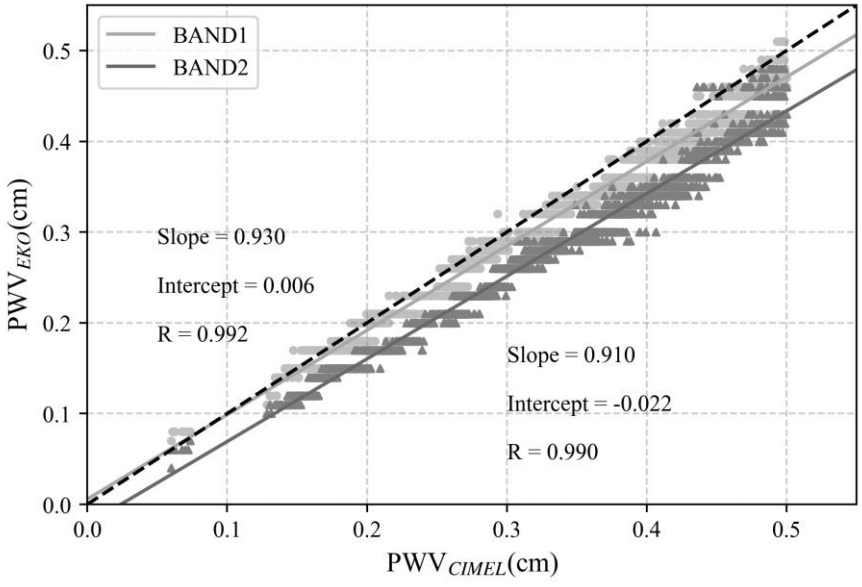

Figure 7. Comparison of water vapor retrieved from BAND1 and BAND2 with PWV_{CIMEL} when PWV_{CIMEL} is less than 0.5 cm.

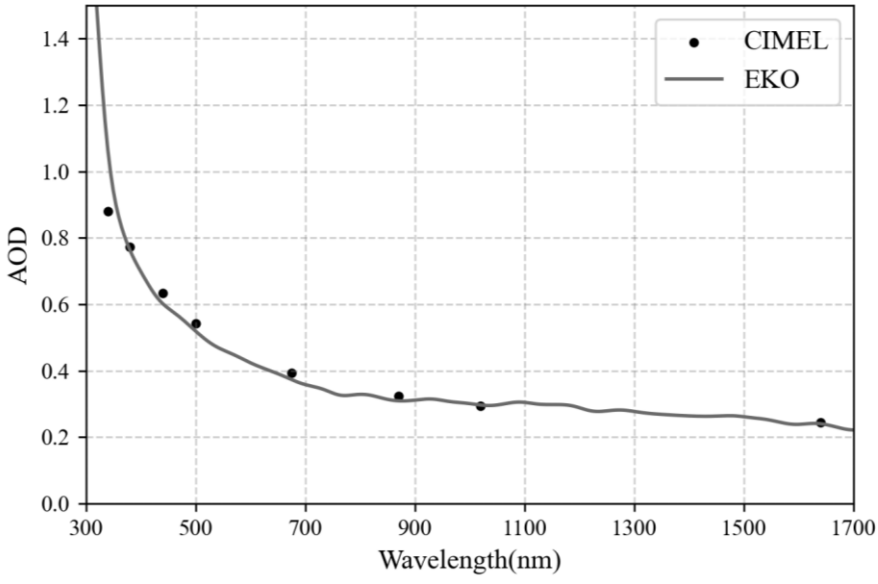

Figure 8. The AOD was retrieved by EKO and provided by AERONET-CIMEL on 06 June 2020 (15:22 UTC+8).

https://doi.org/10.5194/egusphere-2022-315
Preprint. Discussion started: 13 July 2022

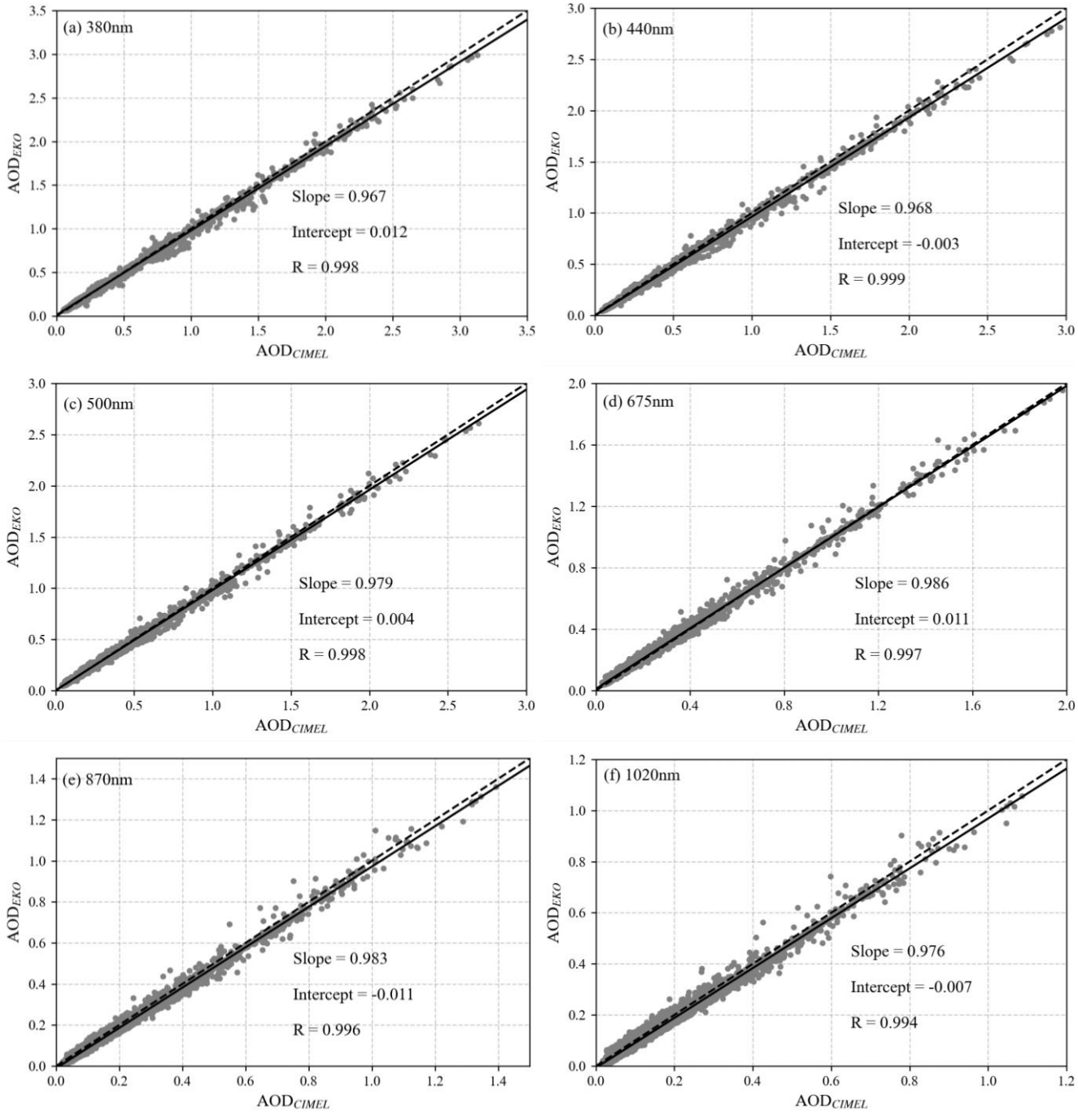

Figure 9. Comparison of AOD_{EKO} versus AOD_{CIMEL} at 380 nm (a), 440 nm (b), 500 nm (c), 675 nm (d), 870 nm (e) and 1020 nm (f) from June 2020 to March 2021 at IAP.

https://doi.org/10.5194/egusphere-2022-315
Preprint. Discussion started: 13 July 2022

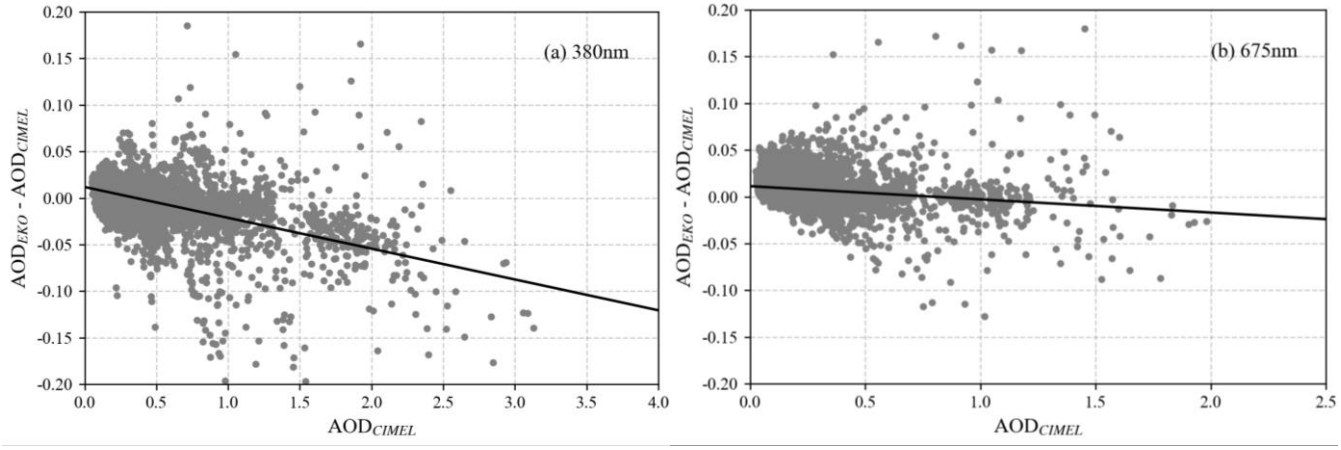

Figure 10. Bias among synchronous AOD_{EKO} and AOD_{CIMEL}, and plotted against AOD_{CIMEL} at 380 nm (a) and 675 nm (b).

https://doi.org/10.5194/egusphere-2022-315
Preprint. Discussion started: 13 July 2022

Table 1 EKO MS711 and MS712 spectroradiometers specifications

Sensor	MS711	MS712
Wavelength	300-1100 nm	900-1700 nm
Wavelength Interval	0.3-0.5 nm	1.2-2.2 nm
Temperature Control	25±2 ℃	-5±0.5 ℃
Dome material	Synthetic Quartz	BK7
Operating conditions	Tem: 0~+40 ℃, Humidity: 0~90 %RH*No condensation	
Spectral Resolution	<7 nm	
Wavelength Accuracy	±0.2 nm	
Exposure Time	10-5000 ms	
Communication	RS-422 / 232C	
Power supply	100-240 VAC, 50/60 Hz	
Field of view (FOV)	5°	

Table 2 Statistics of the comparison between PWV_{EKO} and the PWV_{CIMEL}. (N: number of data, R: Pearson correlation coefficient, Slope: slope of the least squares fit between PWV_{EKO} and PWV_{CIMEL}, RMSE: root mean square error, MB: mean bias, STD: standard deviation).

CIMEL/EKO	BAND	N	R	Slope	RMSE (cm)	MB (cm)	STD (cm)
All data	BAND1	5008	0.999	0.986	0.061 (5.31 %)	-0.027 (-3.57 %)	0.054 (3.93 %)
PWV_{CIMEL}>0.5 cm	BAND1	2977	0.998	0.985	0.077 (4.41 %)	-0.034 (-2.67 %)	0.069 (3.50 %)
PWV_{CIMEL}<0.5 cm	BAND1	2031	0.992	0.930	0.022 (6.41 %)	-0.017 (-4.90 %)	0.014 (4.13 %)
	BAND2	2031	0.990	0.911	0.054 (16.79 %)	-0.051 (-16.26 %)	0.016 (4.17 %)

Table 3 Statistics of the comparison between AOD_{EKO} and AOD_{CIMEL} at 380, 440, 500, 675, 870 and 1020 nm form June 2020 to March 2021 at IAP.

Wavelength (nm)	R	Slope	RMSE	MB	STD
380	0.998	0.967	0.028 (9.16 %)	-0.002 (3.06 %)	0.028 (8.63 %)
440	0.999	0.968	0.029 (7.31 %)	-0.016 (-4.65 %)	0.024 (5.64 %)
500	0.998	0.979	0.021 (7.46 %)	-0.003 (0.69 %)	0.021 (7.42 %)
675	0.997	0.986	0.020 (17.45 %)	0.008 (9.37 %)	0.019 (14.72 %)
870	0.996	0.983	0.021 (20.01 %)	-0.014 (-13.59 %)	0.015 (14.70 %)
1020	0.994	0.976	0.019 (22.06 %)	-0.010 (-11.81 %)	0.016 (18.63 %)